Phase-Transfer-Aided FMNH Production Using Artificial Photosynthesis Cells of Bacterial Type. Cell System Optimization by the Concept of Flux Conjugation

Iwao Tabushi* and Shin-ichi Kugimiya

Contribution from the Department of Synthetic Chemistry, Kyoto University, Sakyo-Ku, Kyoto, 606, Japan. *Received March 20, 1984. Revised Manuscript Received December 4, 1984*

Abstract: Artificial liposomes functionalized with moderately hydrophobic viologens as electron carriers, flavin mononucleotide (FMN) as an electron acceptor, and $Zn{\cdot}T_{SO_3Na}PP$ as a photocatalyst drive very efficient electron flow across the liposomal membrane, giving FMNH in good quantum yields. The FMNH formation is very sensitive to the length of the alkyl chain on the viologens. Optimization of overall electron-transport efficiency is attempted based on the concept of $V^{+}\cdot$ flux conjugation, successfully demonstrating that butylviologen is the best electron carrier. A linear logarithmic relationship was observed between the apparent photon-induced FMNH production and the observed dark phase-transfer-aided electron flow across the liposomal membrane, strongly suggesting that both electron transports are controlled by the same principle, flux conjugation.

Introduction

Energetically uphill reduction of a recyclizable electron acceptor (such as NAD) giving a utilizable reductant and driven by photon irradiation is the essential chemical event involved in the so-called "photoreaction" in *photosynthesis*. The highly efficient charge separation between an electron acceptor and a so-called "photosystem" is of primary importance to the success of the uphill conversion. Nature uses organized assemblies for the highly efficient "overall" charge separation, in which (a) the photosystem(s) is so constructed as to maximize "instantaneous" charge separation, while (b) the electron-transport system is so constructed as to minimize "delayed back-reaction" by minimizing the steady-state concentrations of charge-separated pairs. In accord with this principle, simple mimicking of photosynthesis is achieved by introduction of an interphase, often inducing the efficient "overall" charge separation.[1] The authors have modeled bacterial-type photosynthesis by using a micellar system[1c] or a three-liquid-phase system activated by a detergent,[1b] in which hydrophobic viologens are used as electron-transport catalysts.

The authors now wish to report that artificial liposomes, functionalized with moderately hydrophobic viologens, the electron carriers, promote photochemical "overall" charge separation very efficiently between excited $Zn{\cdot}T_{SO_3Na}PP$ present in an exterior aqueous solution, and FMN present in an interior aqueous solution, or in a system of the reverse topology. It is concluded that "overall" charge separation is aided remarkably by phase transfer of the electron carrier $V^{+}\cdot$, in which the transient $V^{+}\cdot$ concentration gradient generated at the interphase between phase I and II drives interphasial $V^{+}\cdot$ fluxes from phase I to II and further from II to III, minimizing delayed back-reaction in phase I and maximizing the electron fixation in phase III.

Results and Discussions

Preparation of Artificial Photosynthesis Cell of Bacterial Type. The functional liposomes ($FMN^{(i)}|RV^{2+}{\cdot}Lip$) or ($Zn{\cdot}T_{SO_3Na}PP$, $Na_2S_2O_3{}^{(i)}|RV^{2+}{\cdot}Lip$) (R = CH_3, n-C_3H_7, n-C_4H_9, n-C_5H_{11}, n-C_6H_{13}, or n-$C_{10}H_{21}$) (see Figure 1) were prepared as reported elsewhere.[2]

Scheme I. Schematic Representation of Charge-Separation Process

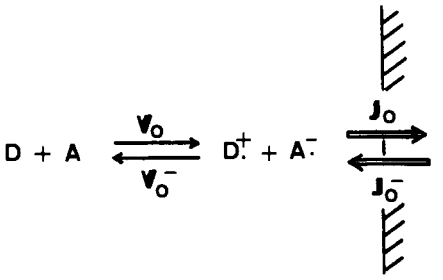

The functionalized liposome solutions (FMN, $RV^{2+(i)}|RV^{2+}{\cdot}Lip|^{(o)}Zn{\cdot}T_{SO_3Na}PP$, $Na_2S_2O_3$, RV^{2+}) or ($Zn{\cdot}T_{SO_3Na}PP$, $Na_2S_2O_3$, $RV^{2+(i)}|RV^{2+}{\cdot}Lip|^{(o)}FMN$, RV^{2+}) (R = CH_3, n-C_3H_7, n-C_4H_9, n-C_5H_{11}, n-C_6H_{13}, or n-$C_{10}H_{21}$) were irradiated at 425 ± 5 nm for selective excitation of $Zn{\cdot}T_{SO_3Na}PP$. Reduction of FMN present in the phase different from the $Zn{\cdot}T_{SO_3Na}PP$ phase proceeded very effectively, giving FMNH as the sole product. This

$$Zn{\cdot}T_{SO_3Na}PP \xrightarrow{h\nu} Zn{\cdot}T_{SO_3Na}PP^{*} \quad \text{(aq phase I)} \quad (1a)$$

$$Zn{\cdot}T_{SO_3Na}PP^{*} + V^{2+} \rightleftarrows Zn{\cdot}T_{SO_3Na}PP^{+}\cdot + V^{+}\cdot \quad \text{(phase I)} \quad (1b)$$

$$Zn{\cdot}T_{SO_3Na}PP^{+}\cdot + S_2O_3{}^{2-} \rightarrow Zn{\cdot}T_{SO_3Na}PP + {}^1/_2S_4O_6{}^{2-} \quad \text{(phase I)} \quad (1c)$$

$$V^{+}\cdot + FNM + H^{+} \rightarrow [V^{2+} + FMN^{-}\cdot + H^{+}] \quad \text{(phase III)} \quad (1d)$$

$$[V^{2+} + FMN + H^{+}] \rightarrow V^{2+} + {}^1/_2FMNH + {}^1/_2FMN \quad \text{(phase III)} \quad (1e)$$

product is protected against "back-reaction" through separation from the potential oxidant temporarily formed in the $Zn{\cdot}T_{SO_3Na}PP$ phase.

Efficiency of Photoinduced Charge Separation Dependent on Surface Area. Charge Separation Aided by Interphasial Transport of Charge (Electron)-Carrying Species. The efficiency of the charge separation in the native photosynthesis systems or related artificial systems is basically described by the competitive, consecutive kinetics of a series of elementary reactions. In an isolated photosystem in a homogeneous medium, overall quantum yield of the charge separation can be reasonably high based on the kinetic design of an optimal redox couple.[3] The charge-separation

(1) (a) For recent reviews, see: Calvin, M. *Acc. Chem. Res.* **1978**, *11*, 369. Fendler, J. H. *Ibid.* **1980**, *13*, 7. Tabushi, I., *Pure Appl. Chem.* **1982**, *54*, 1733. Fendler, J. H. "Membrane Mimetic Chemistry"; Wiley-Interscience: New York, 1982. (b) Tabushi, I.; Yazaki, A.; Koga, N.; Iwasaki, K. *Tetrahedron Lett.* **1980**, *21*, 373. (c) Tabushi, I.; Kugimiya, S.; Mizutani, T. *J. Am. Chem. Soc.* **1983**, *105*, 1658. (d) Ford, W. E.; Otvos, J. W.; Calvin, M. *Nature (London)* **1978**, *274*, 507. (e) Ford, W. E.; Otvos, J. W.; Calvin, M., *Proc. Natl. Acad. Sci. U.S.A.* **1979**, *76*, 3590. (f) Laane, C.; Otvos, J. W.; Ford, W. E., Calvin, M. *Ibid.* **1981**, *78*, 2017. (g) Infelta, P. P.; Grätzel, M.f Fendler, J. H. *J. Am. Chem. Soc.* **1980**, *102*, 1479. (h) Nomura, T.; Escabi-Perez, J. R.; Sunamoto, J.; Fendler, J. H. *Ibid.* **1980**, *102*, 1484. (i) Tunuli, M. S.; Fendler, J. H. *Ibid.* **1981**, *103*, 2507. (j) Lee, L. Y. C.; Hurst, J. K.; Politi, M.; Kurihara, K.; Fendler, J. H. *Ibid.* **1983**, *105*, 370. (k) Hurst, J. K.; Lee, L. Y. C.; Gratzel, M. *Ibid.* **1983**, *105*, 7048. (l) Sudo, Y.; Toda, F. *Nature (London)* **1979**, *279*, 807. (m) Matsuo, T.; Itoh, K.; Takuma, K.; Hashimoto, K.; Nagamura, T. *Chem. Lett.* **1980**, 1009. (n) Brugger, P. A.; Grätzel, M. *J. Am. Chem. Soc.* **1980**, *102*, 2461.

0002-7863/85/1507-1859$01.50/0

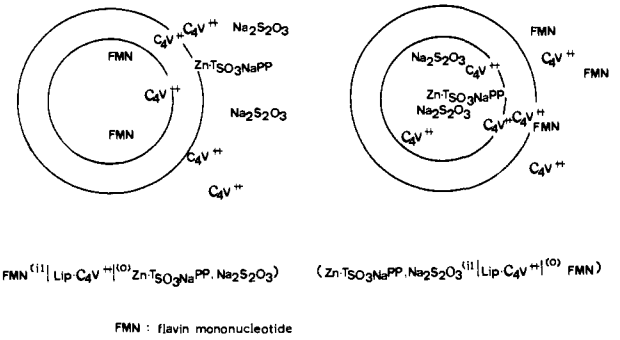

Figure 1. Artificial photosynthesis cells of bacterial type.

efficiency thus determined may be called "intrinsic charge-separation efficiency". This intrinsic charge-separation efficiency is, however, further perturbed by the introduction of an appropriate electron (and/or positive hole) efflux, as shown in Scheme I. The perturbation comes from change in the steady-state concentration of the charge-separated species, which are determined by $\mathbf{V}_0$, $\mathbf{V}_0^-$, $\mathbf{J}_0$, and $\mathbf{J}_0^-$. In the case where $D_0^{+}\cdot$ is not permeable through the

$$\frac{d[A^{-}\cdot]}{dt} = \mathbf{V}_0 - \mathbf{V}_0^- - \mathbf{J}_0 + \mathbf{J}_0^- = \mathbf{V}_0 - \lambda[A^{-}\cdot] + \mathbf{J}_0^- \quad (2)$$

$$[A^{-}\cdot] \text{ steady state} = (\mathbf{V}_0 + \mathbf{J}_0^-)/\lambda$$

membrane, and $\mathbf{V}_0^-$, $\mathbf{J}_0$, $\mathbf{J}_0^-$ are dependent on the $A^{-}\cdot$ concentration, it is clear from eq 2 that larger $\mathbf{J}_0$ makes "back-reaction" ($\mathbf{V}_0^-$) smaller owing to a decrease in the steady-state concentration of $A^{-}\cdot$. Again the total efflux is determined by the electron-transporting capacity of the membrane ($\mathbf{J}_0^0$) as well as the total surface area.

$$\mathbf{J}_0 = \mathbf{J}_0^0 \cdot S_0$$

Therefore, overall quantum yields of the reduction end products (FMNH in the present example) increase by the introduction of appropriately functionalized liposomal membrane, micelle, or any other molecular aggregate, which possibly optimize $\mathbf{J}_0$ through appropriate functionalization.

Artificial Single-Wall Bilayer Lyposome as a Versatile System for Transport Studies. Monolayer or planar bilayers are well characterized and known[4] to be the best systems for the study of a variety of membrane properties. The only serious limitation in using planar systems seems to be their limited surface area, which is directly reflected in limited overall rates of interphasial events such as membrane binding, phase transfer, or transport across the membrane, while cell dynamics of physiological significance is generally very fast as exemplified by stimulus response.[5] Therefore, a remarkable enhancement of overall interphasial rates is necessary to model certain significant cell phenomena, which may be conveniently achieved by (i) an increase in surface area and (ii) an appropriate functionalization. Successful observation of rapid transmembrane proton transport coupled to the rapid transmembrane electron transport through the artificial electron channel of cyt-c_3 is aided by the extremely large surface area of artificial bilayer liposomes (4×10^4 cm^2 for 2 mL of a 1 μM liposomal solution). In this system, the observed proton concentration gradient generated by the coupled proton flux is given by

$$\Delta[H^+] = \frac{\mathbf{J}_{H^+}\Delta t}{V} = \frac{\mathbf{J}_{H^+}{}^0 S \Delta t}{V} \quad (3)$$

where $\mathbf{J}_{H^+}{}^0$ is the coupled proton flux per unit surface area, unit time [$\mathbf{J}_{H^+}{}^0 = f(\mathbf{J}_e{}^0, \Delta[H^+])$], S total surface area, and V volume of the second aqueous phase to which proton is actively transported. Equation 3 demonstrates that $\Delta[H^+]$ becomes larger when the small-size compartments (artificial liposome) are prepared to give large S/V ratios. Transport of electron or any ion is, therefore, best studied by the use of single-wall bilayer artificial liposomes of small diameter.

In the presently studied artificial single-wall liposomes, very efficient, energetically downhill electron transport was observed from excited $T_{SO_3Na}PP\cdot Zn$ (mainly triplet) located in the aqueous phase to FMN located in the aqueous III phase to produce FMNH in good quantum yields (Tabel I). The efficient electron flux is aided by the phase transfer of the electron carriers, viologen cation radicals, which are satisfactorily hydrophobic, but their oxidized form is satisfactorily hydrophilic (Scheme II), as clearly ascertained by distribution experiments.[6]

Two Possible Electron-Transport Mechanisms across Lipid Membrane and Charge Separation at the Artificial Photosystem, $T_{SO_3Na}PP\cdot Zn^{2+}$–Viologen. Artificial liposomes prepared from carefully and freshly purified egg lecithin[2] show very poor electron-transporting properties according to our preliminary experiments, although the partial oxidation of lipids gives relatively high electron-transporting membranes. To facilitate electron transport across the membrane efficiently, there seem to be two types of modifications possible: (i) electron-channel type[2] and (ii) electron-carrier type[6] (Scheme III). Frequently a slow elementary reaction(s) is involved in the "reduction end" like the

Table I. Characteristics of FMNH Production

A. Quantum Yield of FMNH Production[a]

	C_4V^{2+}	C_6V^{2+}
quantum yield, %	10.0	6.4

B.[b] Regeneration of Photocatalyst

$Zn\text{-}T_{SO_3Na}PP$ used	$Zn\text{-}T_{SO_3Na}PP$ recovered	recovered yield
8.0×10^{-9} mol	7.4×10^{-9} mol	92%

C.[b] Regeneration of Electron-Transport Catalyst

C_4V^{2+} used	C_4V^{2+} recovered	recovered yield
1.20×10^{-6} mol	1.15×10^{-6} mol	96%

D.[b] Regeneration of Reduction End[c]

FMN used	FMN recovered	recovered yield
2.52×10^{-7} mol	2.46×10^{-7} mol	97%[c]

[a] [liposome] = 1×10^{-6} M, $[FMN]_o = 1.5 \times 10^{-4}$ M, $[C_4V^{2+}] = 5 \times 10^{-4}$ M, $[Zn\text{-}T_{SO_3Na}PP] = 1.9 \times 10^{-4}$ M, 25 min irradiation. [b] FMNH formation: 1.7×10^{-7} mol, 2 hr irradiation. [c] A small amount (<3%) of unknown product (λ_{max} 360 nm) was obtained after irradiation followed by gel filteration.

Scheme II. Distribution of Alkylviologen Dications and Corresponding Cation Radicals between H_2O–CH_2Cl_2

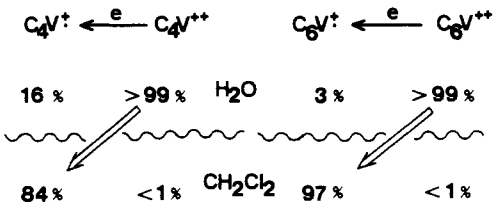

Scheme III. Electron-Transport Mechanism

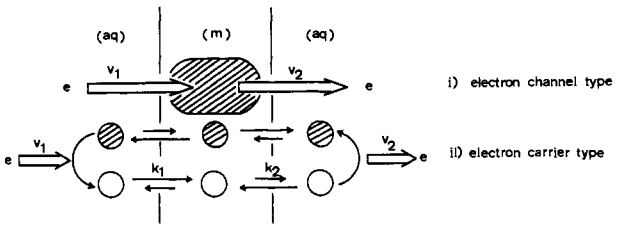

(2) Tabushi, I.; Nishiya, T. *J. Am. Chem. Soc.* **1981**, *103*, 6963; *Tetrahedron Lett.* **1981**, *22*, 4989; *J. Am. Chem. Soc.* **1984**, *106*, 219.
(3) Hiller, R. G.; Goodchild, D. J. "The Biochemistry of Plants"; Hatch, M. D., Boardman, N. K., Eds.; Academic Press: New York, 1981; Vol. 8.
(4) (a) Möbius, D. *Ber Bunsenges. Phys. Chem.* **1978**, *82*, 848. (b) Tien, H. T. "Bilayer Lipid Membrane"; Marcel Dekker: New York, 1974.
(5) Katz, B.; Miledi, R. *Proc. R. Soc. London, Ser. B* **1965**, *161*, 453.
(6) Tabushi, I.; Kugimiya, S. *Tetrahedron Lett.* **1984**, *25*, 3723.

Scheme IV. Schematic Expression of the Simplest Photosynthesis System Having Different Topology

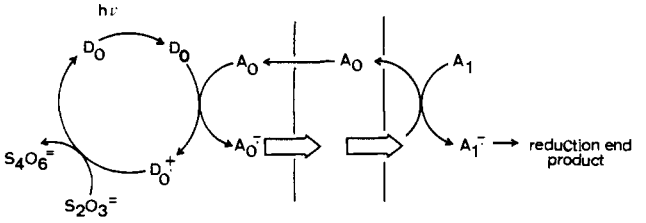

Scheme V. Conjugation between Fluxes

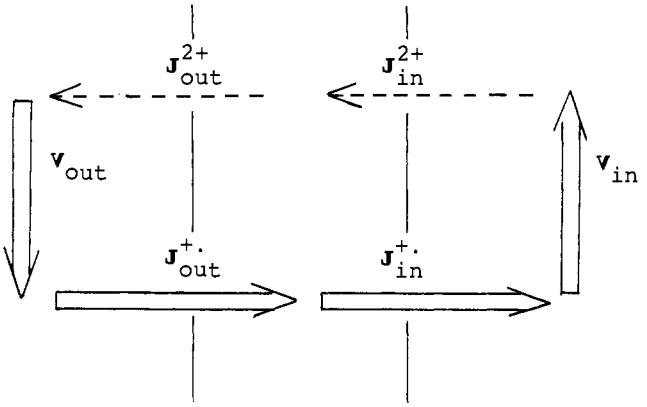

present conversion from FMN to FMNH, and many back-reactions may take place between $A_i^{-}\cdot$ (i = 0, 1, n) and $D_j^{+}\cdot$ (j = 0, 1, m). To minimize the probability of the undesired "cross"

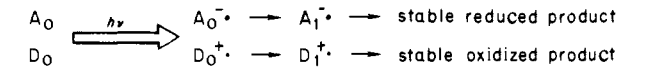

back-reactions, $A_i^{-}\cdot$ and $D_j^{+}\cdot$ are better located in different topologies. This situation is depicted in Scheme IV for the simplest case.

The observed triplet lifetime of $T_{SO_3Na}PP{\cdot}Zn$ (D^{*3}) is 1.1×10^{-3} s, while the observed second-order rate constants of reaction, $D^{*3} + RV^{2+}$ (A_0), and the expected phase-transfer reaction rate of $RV^{+}\cdot$ are 0.9×10^{8} s^{-1} M^{-1} and $10^{-5} - 10^{-4}$ s^{-1} cm^{-2}, respectively, under the present conditions. The oxidation end reaction (eq 5)

$$\underset{(V^{+}\cdot)}{A_0^{-}\cdot} + \underset{(Zn{\cdot}T_{SO_3Na}PP^{+}\cdot)}{D_0^{+}\cdot} \xrightarrow{k_4} \underset{(V^{2+})}{A_0} + \underset{(Zn{\cdot}T_{SO_3Na}PP)}{D_0} \quad (4)$$

$$D_0^{+}\cdot + S_2O_3^{2-} \xrightarrow{k_5} D_0 + {}^1/_2S_4O_6^{2-} \quad (5)$$

has a large rate constant, $k_5 = 1 \times 10^{8}$ s^{-1} M^{-1}, and is capable of suppressing the back-electron-transfer reaction (eq 4) almost completely by simple competition, when the concentration of $S_2O_3^{2-}$ is over 10^{-4} M, under the present condition of $[RV^{+}\cdot] \leq 10^{-6}$ M. Combination of reactions 5 and 6 provides flux of $A_0^{-}\cdot$

$$A_0 + D_0{}^{*3} \xrightarrow{k_6} A_0^{-}\cdot + D_0^{+}\cdot \quad (6)$$

"generated" at the artificial photosystem, when reaction 4 is of little significance. The $A_0^{-}\cdot$ flux thus generated is "conjugated" with the phase-transfer flux as discussed in the following section.

Electron Transport Aided by Phase Transfer of the Electron Carrier, Viologen. When electron flux (in a form of a $V^{+}\cdot$ formation rate, V_{out}, in the present system) is generated in aqueous phase I (exterior) of an artificial liposome system, it can be "conjugated" with an interphasial electron flux, $J_{out}^{+}\cdot$, leading to accumulation of $V^{+}\cdot$ in the liposomal membrane, or to decrease in the $V^{+}\cdot$ concentration in the exterior aqueous phase to suppress undesired side reaction. When an appropriate final electron acceptor is present in phase III (interior aqueous solution), then electron influx $J_{out}^{+}\cdot$ is again "conjugated" with interphasial flux $J_{in}^{+}\cdot$ and further with V_{in} electron flux "converge". Now a new V^{2+} flux "emerges", which is depicted in Scheme V. This conjugation between fluxes at different topology leads to a quasi (short-lived) steady state as shown in eq 7, and the stable steady

$$V_{out} = J_{out}^{+}\cdot = J_{in}^{+}\cdot = V_{in} \quad (7)$$

state, then, is given by eq 8 (see also Figures 2 and 3).

$$V_{out} = J_{out}^{+}\cdot = J_{in}^{+}\cdot = V_{in} = J_{in}^{2+} = J_{out}^{2+} \quad (8)$$

The "conjugated" electron flux in the present artificial cell of bacterial, type has the following characteristics under the typical experimental conditions listed (see also Table I).

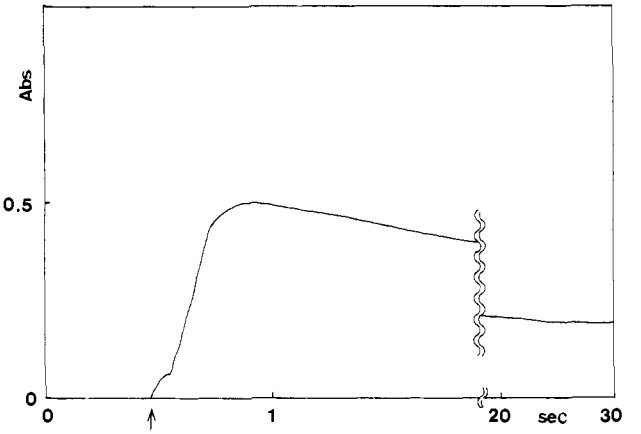

Figure 2. Short-lived steady state and stable steady state of the electron-transport reactionin the dark, after the addition of aqueous $S_2O_4^{2-}$ (at the arrow), monitored at 605 nm, characteristic absorption of viologen cation radical: [liposome] = 1×10^{-6} M, total outer surface area is calculated to about 4×10^{4} cm, $[C_4V^{2+}]_0 = 5.5 \times 10^{-5}$ M, $[FMN]_i$ = 19 mM, $[Na_2S_2O_4]_0 = 6.5 \times 10^{-4}$ M, pH 6.8, 25 °C.

Table II. Photochemical Properties of Photocatalyst in the Presence of Alkylviologens

A. Lifetime of $^{S}Zn{\cdot}T_{SO_3Na}PP$

alkylviologens (M)	τ_S (ns)	ref
none	1.70	10
C_4V^{2+}, 0.79×10^{-4}	1.83	this work[b]
C_4V^{2+}, 5.5×10^{-4}	1.41 (55%)[a]	this work[b]

B. Deactivation of $^{T}Zn{\cdot}T_{SO_3Na}PP$ with Alkylviologens

lipid–alkylviologens (M)	k_Q (M^{-1} s^{-1})	ref
lecithin-C_4V^{2+}, 1.58×10^{-4}	0.95×10^{8}	this work[c]
DHP–C_4V^{2+}, 0.7×10^{-4}	25×10^{8}	1k
DHP–$C_{14}C_4V^{2+}$, 0.7×10^{-4}	2.4×10^{8}	1k

[a] Biphasic decay curve, slower process 45%. [b] Excitation at 425 nm and monitored at 540–800 nm with a SC-54 filter (Fuji), phosphate buffer (pH 6.8), 26 °C. [c] Excitation at 590 nm, monitored at 745 nm, $[Zn{\cdot}T_{SO_3Na}PP] = 1.5 \times 10^{-4}$ M (pH 6.8).

Table III. Quantum Yield of FMNH Production[a]

	A	B	C[a]	D[a]	E[a]
chemical yield, %	95	95			
quantum yield, %	10	3	3.8×10^{-2}	0.44	2.4
reference			1e	1f	1i

[a] Yield of viologen radicals: (A) $(Zn{\cdot}T_{SO_3Na}PP, Na_2S_2O_3{}^{(i)}|LiP{\cdot}C_4V^{2+}|^{(o)}FMN)$; (B) $(FMN^{(i)}|Lip{\cdot}C_4V^{2+}|^{(o)}Zn{\cdot}T_{SO_3Na}PP, Na_2S_2O_3)$; (C) (EDTA, $Lip{\cdot}Ru^{2+}|^{(o)}C_7V^{2+}$, Zn^{2+}); (D) (EDTA, $K^{+}|^{(i)}Lip{\cdot}Ru^{2+}$, $Val|^{(o)}C_7V^{2+}$, K^{+}); (E) $(MeV^{2+(i)}|^{-}Lip^{-}|^{(o)}Ru^{2+}$, EDTA).

Table IV. Recycling Number of Catalysts

	A		B	
	$Zn{\cdot}T_{SO_3Na}PP$	C_4V^{2+}	$Zn{\cdot}T_{SO_3Na}PP$	C_4V^{2+}
obsd recycling[a]	120	30	2.5	1.4
theor recycling[b]	8×10^{3}	2×10^{2}	30	1.5×10^{2}

[a] Mol of the final product formed/number of the catalyst used. [b] Mol of the final product formed/number of the catalyst destroyed.

Table V. Association and Dissociation Rate Constants for Viologen Cation Radical–Liposome Complex[a]

alkyl viologen	rate constant k_{assoc} (s^{-1} cm^{-2}) β-naphthol	anthracene	k_{diss} (s^{-1} cm^{-2})
$C_2V^{+\cdot}$	$(7.6 \pm 0.8) \times 10^{-5}$	16×10^{-5}	$(1.6 \pm 0.2) \times 10^{-4}$
$C_4V^{+\cdot}$	$(4.0 \pm 1.0) \times 10^{-5}$		$(2.9 \pm 0.6) \times 10^{-5}$
$C_6V^{+\cdot}$	$(3.5 \pm 2.0) \times 10^{-5}$	3.5×10^{-5}	$(1.3 \pm 0.4) \times 10^{-6}$

[a] [liposome] = 1×10^{-6} M, surface area = 4×10^4 cm^2, $[V^+] = 2.0 \times 10^{-5}$ M, 25 °C, [β-naphthol] = 5×10^{-5} M, excitation at 335 nm, emission at 355 nm; [anthracene] = 1.4×10^{-5} M, excitation at 355 nm, emission at 404 nm.

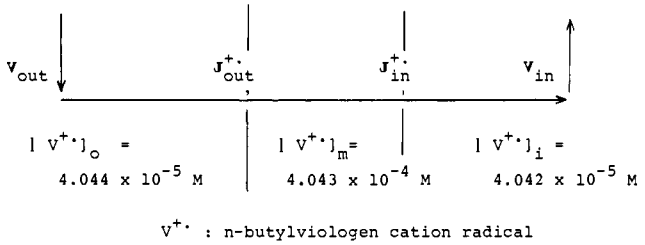

Figure 3. Viologen cation-radical concentrations at the photocenter phase and membrane based on the flux conjugation at the unstable steady state.

Flux Generation and Flux Convergence of Viologen Cation Radical in Artificial Photosynthesis Cell. In the present liposome system described in eq 9, the flux of $V^{+\cdot}$ is generated at the

$$(FMN, V^{2+(o)}|V^{2+}|^{(i)}\ V^{2+}, Zn\text{-}T_{SO_3Na}PP, Na_2S_2O_3) \quad (9a)$$

$$(Zn\text{-}T_{SO_3Na}PP, Na_2S_2O_3, V^{2+(o)}|V^{2+}|^{(i)}V^{2+}, FMN) \quad (9b)$$

artificial photocenter, $Zn\text{-}T_{SO_3Na}PP$, by irradiation (425 nm). Photochemical characteristics of the present photocenter were neither affected by viologen nor by liposome seriously as shown by the observed "normal" singlet lifetime of $Zn\text{-}T_{SO_3Na}PP$ or the triplet quantum yield (Table II). Electron-transfer rates from the triplet photocenter to viologen were measured at the characteristic triplet absorption (745 nm). The observed second-order rate constants are of comparable magnitude with methylviologen or methyltetradecylviologen (see Table II). Therefore, the observed flux generation of viologen cation radical is not seriously affected by the present membrane. The flux convergence rates of viologen cation radical at the artificial reduction end were also measured in an isolated system.

The phase-transfer fluxes are independently measured in two-phase systems. A part of our preliminary measurements of phase-transfer rate constants are listed in Table V. An example of independent flux rate measurements is shown below for $J_{out}^{+\cdot}$. Exterior phase-transfer flux is given by

$$J_{out}^{+\cdot} = k_{0\rightarrow m}[V^{+\cdot}]_0 S_0 - k_{m\rightarrow 0}[V^{+\cdot}]_m S_0$$

where rate constants $K_{0\rightarrow m}$ are obtained by rapid mixing of an aqueous $V^{+\cdot}$ solution with a solution of liposome containing either 1-naphthol or anthracene as a fluorescence probe in the hydrophobic core. Then fluorescence quenching rates are measured, while rate constant $k_{m\rightarrow 0}$ is obtained from $k_{0\rightarrow m}$ and the two-phase equilibrium constant, $K = k_{0\rightarrow m}/k_{m\rightarrow 0}$, is independently measured.

The steady-state concentration of $(V^{+\cdot})_T$ (see Figure 3) calculated from eq 7 by use of rate constants independent measured is in a good agreement with the observed value.

The interphasial fluxes (conjugation fluxes) are driven by the potential gradient temporarily applied at the interphases, that is, simply produced by (i) overloading of $V^{+\cdot}$ at the photocenter, (ii) overconsumption of $V^{+\cdot}$ at the reduction end, and (iii) limited rates of the phase transfer at the interphases.

Based on the information obtained from independent measurements, it may be safely concluded that all or a major part, at least, of electron transport is achieved via the phase-transfer-flux conjugation mechanism.

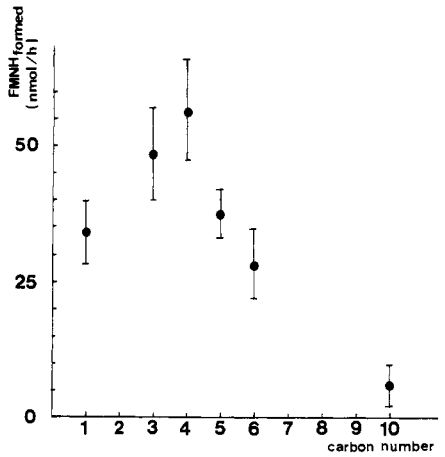

Figure 4. Overall quantum yield of FMNH production vs. alkyl chain length of the catalysts.

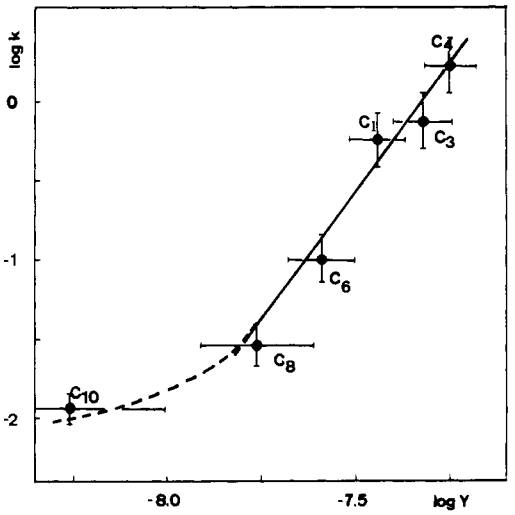

Figure 5. Photoinduced electron transport vs. dark electron transport: Y = quantum yield of FMNH production; k = electron-transport rate constant.

Total Efficiency of Artificial Photosynthesis Systems of Bacterial Type. Regeneration of Photosystem, Electron Carrier, or Reduction End and Quantum Yield. The present flux conjugation system gave satisfactorily overall quantum yield of FMNH (see Table I). In reasonably high $S_2O_3^{2-}$ concentration, other side reactions destroying the porphyrin cation radical hardly compete with the regeneration reaction, affording a very high recycling number of 250 for the porphyrin·Zn^{2+} complex. The yield of FMNH based on the consumed FMN was nearly quantitative, as determined by the electronic spectrum. When FMNH was reoxidized with O_2, FMN was recovered again in nearly quantitative yield as determined spectroscopically (see Table I).

Recycling of the electron carrier, RV^{2+}, during the overall photosynthesis reaction was determined under the conditions where the total amount of RV^{2+} was much smaller than the total amount of $S_2O_3^{2-}$ and FMN (see Table I). The recycling number (number of electrons fixed/number of RV^{2+} molecules destroyed) was found to be very high in the presence of a relatively hydrophobic anion such as Br^-. However, it was ascertained by the independent experiments that in the absence of any appropriate counteranion, $S_2O_4^{2-}$ or $S_2O_3^{2-}$ goes to the membrane with viologen cation radical, where further reduction proceeds irreversibly and quite rapidly. The recycling characteristics of the present artificial photosynthesis system are summarized in Table I.

The observed overall quantum yield of FMNH production showed a characteristic biphasic dependence on the hydrophobicity or the alkyl chain length (Figure 4), in which the optimal flux conjugation takes place at C_4, similarly to dark electron transport.[10] Fairly good linear correlation between dark electron transport and

the present photoinduced electron transport shown in Figure 5 strongly suggests that both electron transports are mainly controlled by the same principle, the proposed flux conjugation.

Experimental Section

Instruments. Electronic absorption spectra were measured with either a Union SM-401 high-sensitivity spectrometer or a Hitachi 340S spectrophotometer. Fluorescence spectra were measured with a Union FS-301 high-sensitivity fluorescence spectrometer. Sonication was performed with an ultrasonic disruptor, Model UR-200P (Tomy Seiko). Centrifugation was carried out with a refrigerated centrifuge, Tomy Seiko Model RS-20III. Steady-state irradiation was carried out using a WACOM 500-W xenon lamp in conjunction with a grating monochromator (1200 grooves/nm) (Shimadzu, Bausch & Lomb). Fluorescence lifetimes were measured with a Horiba NAES-1100 equipped with a 540-nm cut-off filter (SC-54, Fuji). Flash photolysis studies were carried out using a Model DL-2100 C dye laser (Phase-R) and a RA-1200 (Union) detector. Rapid reactions in the dark were recorded with a stopped-flow spectrophotometer, Union RA 401, at 25 °C under Ar atmosphere.

Materials. Commercially available reagents were used without further purification except otherwise stated. Egg yolk lecithin was carefully purified according to the literature method.[7] $Zn\text{-}T_{SO_3Na}PP$ and alkylviologen dications were prepared as described previously.[8] All solutions used in the present study were deaerated using a sequence of evacuation and argon back-flushing in an ice bath (the procedure was repeated 20 times per sample).

Preparation of Artificial Single-Wall Bllayer Liposomes. Artificial lecithin liposomes containing FMN and C_4V^{2+} in its interior aqueous solution were prepared according to a slight modification of our previously reported procedure.[2]

A solution of 100 mg of carefully purified egg yolk lecithin[2] and 10 mg of C_4V^{2+} in 5 mL of CH_2Cl_2 was gently evaporated under reduced pressure under Ar. Into the resulting lecithin thin layer film a solution of 200 mg of FMN in 5 mL of 50 mM phosphate buffer (pH 6.8) was added, and the lecithin film was suspended in the solution. The suspension was sonicated in an ice bath in an Ar box for 3 min followed by further sonification for 2 min. The procedure was repeated five times. The resulting solutionwas centrifuged (1.8×10^4 rpm) for 30 min at 4 °C. The supernatant was applied to Sepharose 4B column (1.6 cmϕ × 35 cm) and eluted with 50 mM phosphate buffer (pH 6.8) at 6 °C. Single-wall bilayer liposomes were obtained after an elution volume of 42 to 54 mL had passed.

Artificial liposomes containing $Zn\text{-}T_{SO_3Na}PP$, $Na_2S_2O_3$, and C_4V^{2+} in the interior aqueous phase were prepared by a procedure similar to that described above for FMN and C_4V^{2+} containing liposomes.

Determination of the Quantum Yield for the Formation of FMNH. The quantum yield for the formation of FMNH in the artificial liposome, under conditions of steady-state photolysis, was determined using ferrioxalate actinometry.[9] Both incident and transmitted light were measured at 22 °C using 0.1 mol of ferrioxalate solution (2 cm depth). An unmodified liposome solution was used as a reference.

Steady-State Photolysis. The deaerated liposome solutions in 10-mm quartz cells were irradiated with a 500-W xenon lamp equipped with a grating monochromator (1200 grooves/nm) (425 ± 5 nm). Reduction of FMN was followed spectrophotometrically (by monitoring change in absorbance of between 300 and 500 nm).

Typical Procedure of the $Na_2S_2O_4$ Reduction of FMN Present in the Interior Aqueous Solution of the Functionalized Liposome (FMN, $C_4V^{2+(i)}|Lip\text{-}C_4V^{2+}$). A freshly prepared liposome solution (1.5 mL) (FMN, $C_4V^{2+(i)}|Lip\text{-}C_4V^{2+}$), kept at pH 6.8 with a 5 mM phosphate buffer containing 45 mM sodium bromide, was placed in a 10-mm quartz cell equipped with a three-way stopcock. Into this solution 0.5 mL of a 0.1 mM solution of C_4V^{2+} was added. The solution was deaerated as described earlier, and into the deaerated liposome solution, at 25 °C, 0.2 mL of a freshly prepared $Na_2S_2O_4$ solution (7.1 mM) (by titration with K_3FeCN_6(aq)) was added using a specially designed syringe.[2] Reduction of the internal FMN and formation/consumption of $C_4V^{+\cdot}$ were followed by monitoring the changes in absorbance at 450 and 605 nm, respectively.

Registry No. CH_3V^{2+}, 4685-14-7; $C_3H_7V^{2+}$, 46903-41-7; $C_4H_9V^{2+}$, 47082-19-9; $C_5H_{11}V^{2+}$, 47230-70-6; $C_6H_{13}V^{2+}$, 47369-13-1; $C_{10}H_{21}V^{2+}$, 47709-85-3; FMN, 146-17-8; FMNH, 5666-16-0; $Zn\text{-}TSO_3NaPP$, 80004-36-0; H^+, 12408-02-5; $Na_2S_2O_4$, 7775-14-6.

(7) Singleton, W. S.; Gray, M. S.; Srown, M. L.; White, J. L. *J. Am. Oil. Chem. Soc.* **1965**, *42*, 53.

(8) Tabushi, I.; Yazaki, A. *Tetrahedron* **1981**, *37*, 4185.

(9) $\phi_{425} = (2[FMNH]_{formed}{}^a/[h\nu]_{absd}) = 2[FMNH]_{formed}/\{[modified\ Lip]_{absd}{}^b - [unmodified\ Lip]_{absd}{}^{b,c}\}$: ^{a}*Based* on UV determination (FMN: $\epsilon_{316} = 2.7 \times 10^3$, $\epsilon_{370} = 1.2 \times 10^4$, $\epsilon_{470} = 1.05 \times 10^4$. FMNH: $\epsilon_{316} = 7.4 \times 10^3$, $\epsilon_{370} = 3.9 \times 10^3$, $\epsilon_{470} = 7 \times 10^2$). ^{b}*Chemical* Actinometry using ferrioxalate. ^{c}*Light* diffraction.

(10) Kalyanasundaram, K.; Neumann-Spallart, M. *J. Phys. Chem.* **1982**, *86*, 5163.

Gas-Phase Ion Decompositions Occurring Remote to a Charge Site

Nancy J. Jensen, Kenneth B. Tomer, and Michael L. Gross*

Contribution from the Midwest Center for Mass Spectrometry, Chemistry Department, University of Nebraska—Lincoln, Lincoln, Nebraska 68588. *Received September 4, 1984*

Abstract: Several classes of closed-shell, gas-phase ions have been found to decompose upon collisional activation in a manner which does not rely on charge initiation. The reactions provide specific and highly informative structural information. This type of fragmentation, which was observed first in a study of carboxylate anions of unsaturated fatty acids, is now identified as parallel losses of the elements of C_nH_{2n+2} initiated from the alkyl terminus. A homologous series of saturated fatty acid anions ranging in chain length from 5 to 18 carbons has been used as a model system to characterize the phenomenon. The fragmentation occurs also for collisionally activated sulfate and sulfonate anions and long-chained amine and phosphonium cations. Deuterium labeling was used to determine that the C_nH_{2n+2} losses are from the alkyl terminus and that a probable mechanism is a process which involves a 1,4 hydrogen elimination with subsequent formation of terminally unsaturated carboxylate anions and neutral olefins.

The mechanisms of decomposition of gas-phase ions such as those which are produced in a mass spectrometer have been explained in terms of charge-site or radical-site initiation.[1,2] The role of charge site is particularly well accepted for fragmentations of radical cations produced by electron or photon impact. The McLafferty rearrangement is illustrative. Hydrogen transfer takes

(1) McLafferty, F. W. "Interpretation of Mass Spectra"; University Science Books: Mill Valley, CA, 1980; pp 45-74.

(2) Williams, D. H.; Howe, I. "Principles of Organic Mass Spectrometry"; McGraw Hill: London, 1972; pp 94-121.

0002-7863/85/1507-1863$01.50/0